J Mater Sci (2008) 43:7426–7431
DOI 10.1007/s10853-008-2725-8

ULTRAFINE-GRAINED MATERIALS

Crack growth in ultrafine-grained AA6063 produced by equal-channel angular pressing

Lothar W. Meyer · Kristin Sommer · Thorsten Halle · Matthias Hockauf

Received: 7 March 2008 / Accepted: 12 May 2008 / Published online: 26 July 2008

Abstract Crack growth behaviour of ultrafine-grained AA6063, processed by equal-channel angular pressing (ECAP) via route E at room temperature, was evaluated with special emphasis on the effect of grain size distribution and work hardening. A bimodal, two times ECAPed condition and a monomodal ultrafine-grained condition after eight ECAP passes are compared with the coarse grained peak aged material. Depending on their microstructure, the ECAPed materials show significantly lower fatigue threshold values (ΔK_{th}) and higher crack growth rates (da/dN) than their coarse grained counterparts. Micrographs of the crack propagation surfaces reveal the reduced grain size as major key to increased crack growth rates of the ECAPed material, as it influences roughness-induced crack closure and crack deflections. Furthermore, the effects of other features, such as ductility, work hardening capability and grain boundary characteristics, are discussed.

Introduction

Methods of severe plastic deformation (SPD), such as equal-channel angular pressing (ECAP), have become more and more established as a powerful tool for improving a bulk material's strength and reducing its grain size down to the submicron range [1, 2]. Extensive studies have been conducted on strength and ductility properties of different SPD materials, further continuing with investigations on fatigue behaviour in the low (LCF) and high cycle fatigue (HCF) range [3–6]. It has been found that the material's improved strength leads to an enhanced high cycle fatigue (HCF) life. In turn, the high degree of strain hardening in the as-processed condition results in a significantly reduced ductility, which consequently leads to a drastic impairment of low cycle fatigue (LCF) properties.

In conjunction with fatigue life experiments, the characterisation of crack initiation and growth in ultrafine-grained (UFG) materials has become a subject of increasing interest. Vinogradov et al. [7, 8] have clearly shown that an ECAP-processed UFG material generally exhibits the same stages of crack propagation as a conventional coarse grained (CG) material: (I) a near-threshold region of slow crack advance at a low stress intensity factor range ΔK, (II) an intermediate stage which can be described by the well-known Paris–Erdogan-equation

$$\frac{da}{dN} = C(\Delta K)^m \tag{1}$$

and (III) the stage of unstable crack growth at high ΔK. Compared to their CG counterparts, the UFG microstructures showed a lower fatigue threshold ΔK_{th} and higher crack growth rates da/dN, especially in the near-threshold region. This behaviour has been attributed to a less tortuous crack path and, in conjunction with this, to a less intensive roughness-induced crack closure [9, 10]. For crack growth in materials with conventional grain size, such an interrelation between smaller grain size and higher crack growth rate is already well established [11]. Contrary to this, it is worth mentioning that in several investigations [7, 8, 10], at higher ΔK the crack growth rate in the UFG material was observed to be lower than in the CG material. However, this phenomenon has not been explained thoroughly, yet. Besides the

L. W. Meyer · K. Sommer (✉) · T. Halle · M. Hockauf
Institute of Materials and Impact Engineering, Chemnitz University of Technology, Erfenschlager Str. 73, 09125 Chemnitz, Germany
e-mail: kristin.sommer@mb.tu-chemnitz.de

reduced grain size of SPD materials, their reduced ductility, caused by the strongly diminished strain hardening capability, is also supposed to have a derogating influence on crack growth behaviour. This is because, similar to LCF behaviour, fatigue crack growth is also associated with relatively large cyclic strains and plastic deformation in the vicinity of the crack tip [8]. In our study crack growth behaviour in two different ECAP-processed microstructures are compared with the initial coarse grained condition to investigate the influence of grain size distribution. These conditions have been chosen based on a detailed study on the development of the microstructure during repetitive ECAP passes [12]. A homogenous, completely refined microstructure, obtained by processing with a high number of ECAP passes and a condition subjected to only two passes, which resulted in a partly refined, bimodal microstructure, have been chosen for investigation.

Experimental methods

For the present investigation, a commercially extruded aluminium wrought alloy AA6063 in the peak aged condition T6 was used. The chemical composition is given in Table 1. Repetitive ECAP processing was conducted at room temperature (RT) in a die with two square channels intersecting in a 90° angle. Billets of 15 × 15 mm^2 in cross section were pressed for two and eight passes, following route E. This route represents a 180° rotation about the extrusion axis after an odd number of passes and a 90° clockwise rotation about the extrusion axis after an even number of passes [13]. Following this route, an effective microstructural breakdown with a high fraction of fully worked volume, especially for billets with short aspect ratios, is achieved. According to [14], with the used channel angle of 90°, the equivalent strain for two and eight pressings is 2.3 and 9.1, respectively. Tensile tests were conducted at an initial strain rate of 10^{-3} s^{-1}, using round specimens with a diameter of 3.5 mm and a gauge length of 10.5 mm. For fatigue crack propagation measurements, single edge bend (SEB) specimens with a geometry according to ASTM E399 [15] and a thickness of 6.5 mm were used. Crack length was measured continuously with crack measurement foils, working according to the principle of indirect electric potential measurement. Fatigue crack growth experiments were carried out ΔK-controlled in a "RUMUL" resonant testing machine, applying a constant load ratio of $R = K_{min}/K_{max} = 0.1$. After precracking at $\Delta K \sim 5$ $MPam^{1/2}$, the cyclic stress intensity factor was lowered in small steps, until the threshold value ΔK_{th} was reached. Afterwards, ΔK was increased again in small steps, beginning from $\Delta K \approx 3$ $MPam^{1/2}$. With this procedure, crack growth rates could be measured without any load history effect from the threshold region up to a cyclic stress intensity of about 20 $MPam^{1/2}$. Figure 1 shows the position of the SEB specimen as it was taken from the ECAP billet; the direction of crack growth in relation to the shear plane of the last ECAP pass is marked with an arrow. Microstructural investigations were performed by electron backscatter diffraction (EBSD) on disks taken from the flow plane, parallel to the direction of pressing. For documentation of the crack growth surfaces, Scanning electron microscopy (SEM) micrographs were taken in a "LEO 1455VP".

Table 1 Chemical composition (wt.%) of the investigated aluminium alloy

Designation	Mg	Si	Fe	Mn, Zn, Cu	Al
AA6063	0.52	0.43	0.16	<0.01	Balance

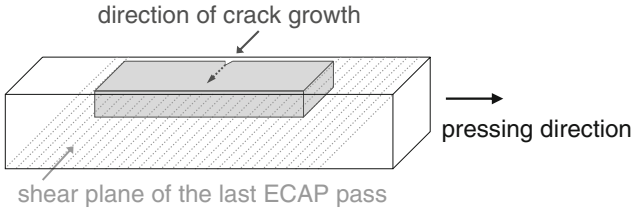

Fig. 1 Position of SEB specimen within ECAP billet

Results and discussion

Microstructure and tensile properties

For the investigated material, detailed studies on the microstructural development at successive ECP processing have been conducted previously [12]. In this section, only a brief discussion on the relevant microstructural features will be presented. As grain size and grain size distribution are seen as important factors influencing the crack growth behaviour, these parameters will be pictured in the following. Figure 2 shows EBSD orientation maps of the conditions under investigation. High angle grain boundaries (HABs) with a misorientation angle ≥15° are marked as black lines.

The initial material consists of coarse globular grains with an average size of about 100 μm. In the material after two passes, those grains are elongated in the directions of macroscopic shear during ECAP. Furthermore, in this microstructure, microshear bands are present, consisting of numerous very small equiaxed subgrains. These bands have widths of about 0.5–1 μm and are characterised by a high misorientation angle towards the surrounding matrix. Since the ECAP shear plane for the first and second pass

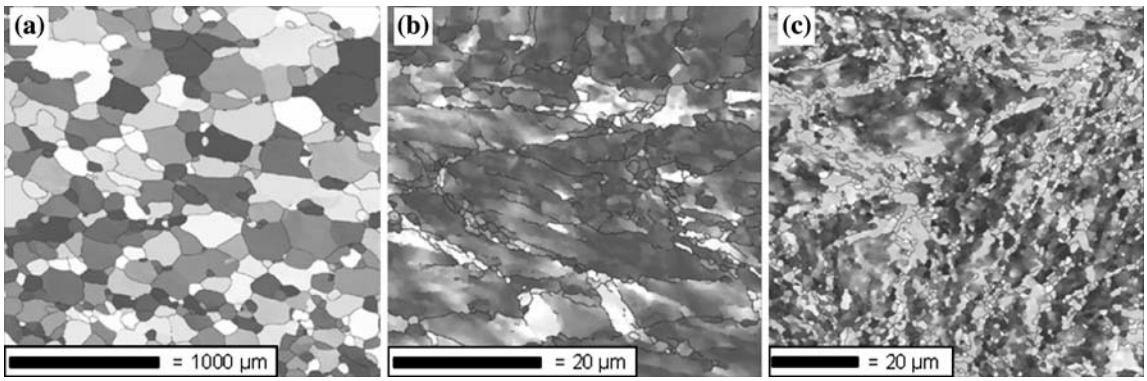

Fig. 2 EBSD investigations of the material's microstructure (**a**) in the initial CG condition, (**b**) after 2 ECAP passes and (**c**) after 8 ECAP passes

was identical for the applied processing route, this bimodal grain size distribution remains up to the second pass.

After eight passes, the material was worked along four different orthogonal ECAP shear planes and is completely pervaded by microshear bands. In this state, the microstructure can be considered as homogeneously refined, completely consisting of ultrafine grains with a grain size in the range of 1 µm and smaller. As described in [12], during repetitive pressing LABs, which are introduced during the first passes, are successively converted into HABs.

The materials' strength and ductility was characterised by tensile tests. According to Fig. 3, ECAP processing at RT leads to a significant increase, both in yield strength and ultimate tensile strength, when compared to the CG initial condition. This behaviour is caused by the effect of severe strain hardening in combination with a grain refinement due to the formation of subcells, as reported numerously [1–6]. A number of two passes results in an increase in yield strength of about 51% compared to the peak aged CG condition. During further processing, the strengthening effect becomes less pronounced, leading to an increase in yield strength of 72% for the material after eight passes. It can be seen from the tensile test curves that the ductility is decreased significantly for the as-processed conditions. With a uniform elongation (UE) of only about 1%, those materials' strain hardening capability has been almost exhausted during SPD processing. Nevertheless, the UE and elongation to failure are slightly higher for the material after eight passes than after two passes. This behaviour is explained with the change in grain boundary characteristics during repetitive pressing. It is assumed that the increased amount of HABs extenuates the materials' susceptibility to early strain localisation [9, 12].

Crack growth behaviour

Fatigue crack growth behaviour of the conditions under investigation is presented in Fig. 4. Coefficients of the Paris–Erdogan-equation, describing crack growth in stage II, and fatigue thresholds are given in Table 2.

Both the initial CG material when compared to the as-processed conditions and the two different SPD conditions among each other show strong differences in crack growth

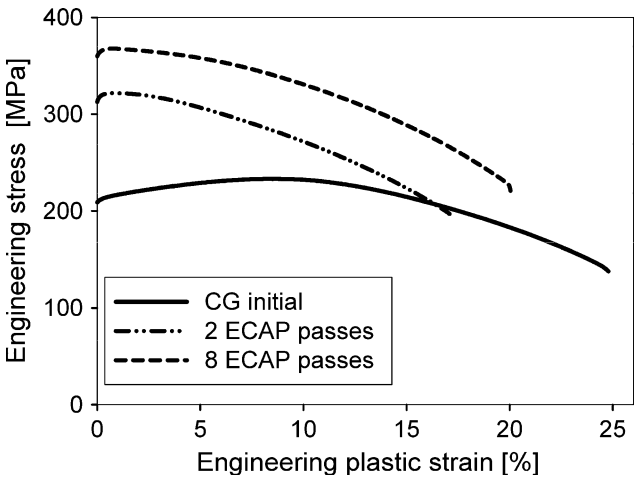

Fig. 3 Tensile properties

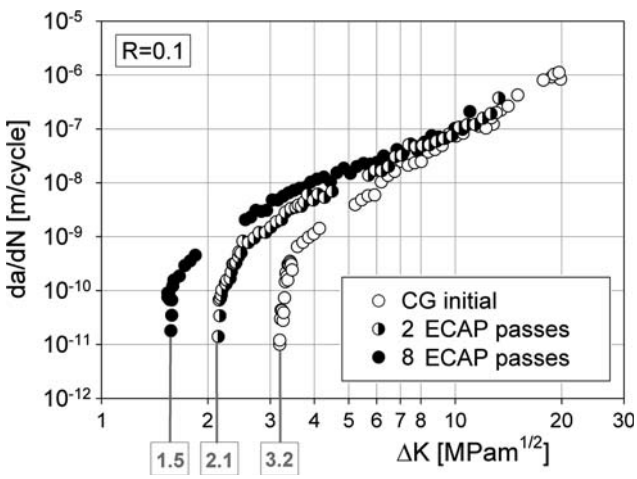

Fig. 4 Fatigue crack growth behaviour

Table 2 Coefficients of Paris–Erdogan-equation $da/dN = C(\Delta K)^m$ and fatigue threshold, for $R = 0.1$

Condition	C (m/cycle)	m	ΔK_{th} (MPam$^{1/2}$)
CG initial (T6)	2.664×10^{-12}	4.394	3.2
2 ECAP passes	5.787×10^{-11}	3.128	2.1
8 ECAP passes	1.028×10^{-10}	3.018	1.5

behaviour. The CG condition exhibits the highest fatigue threshold and the lowest crack propagation rate. This behaviour is mainly attributed to its coarse grains, which cause a strong deflection of the crack path, and therewith a high amount of energy consumption for crack propagation. For both UFG materials, thresholds are lower and crack propagation rates are higher. Nevertheless, especially at low stress intensities, clear distinctions are evident when comparing the homogeneous and the bimodal UFG conditions. Presumably due to its fraction of remaining fragments of coarse grains, the bimodal condition shows an explicitly higher threshold when compared to the homogeneous UFG condition. Above the near-threshold region, fatigue crack growth behaviour of the bimodal condition exhibits an intermediate characteristic, but tends more towards the homogenous UFG condition for higher crack growth rates. For crack growth rates above 10 MPam$^{1/2}$, differences in crack growth rates of the different conditions become less obvious. It is important to note that this impression is supported by the double logarithmic graph scaling.

The SEM images of the crack propagation surfaces shown in Fig. 5 give a descriptive insight into crack propagation features and the underlying microstructure. To ensure comparability, all images show surfaces of crack propagation at the same stress intensity factor range of 7 MPam$^{1/2}$. On the surfaces, grain shapes of the underlying microstructure can be perceived, which give indication for the occurrence of intergranular cracking, as it is the dominant mode in polycrystals fatigued at intermediate or high strain amplitudes [16, 17].

When analysing SPD materials concerning grain size, also the grain boundary characteristics, such as misorientation angles between adjacent grains have to be considered, because the size of subgrains formed by LABs might be significantly smaller than the size of grains bordered by HABs. As shown in [18], fatigue cracks initiate and propagate preferably along HABs, since they comprise

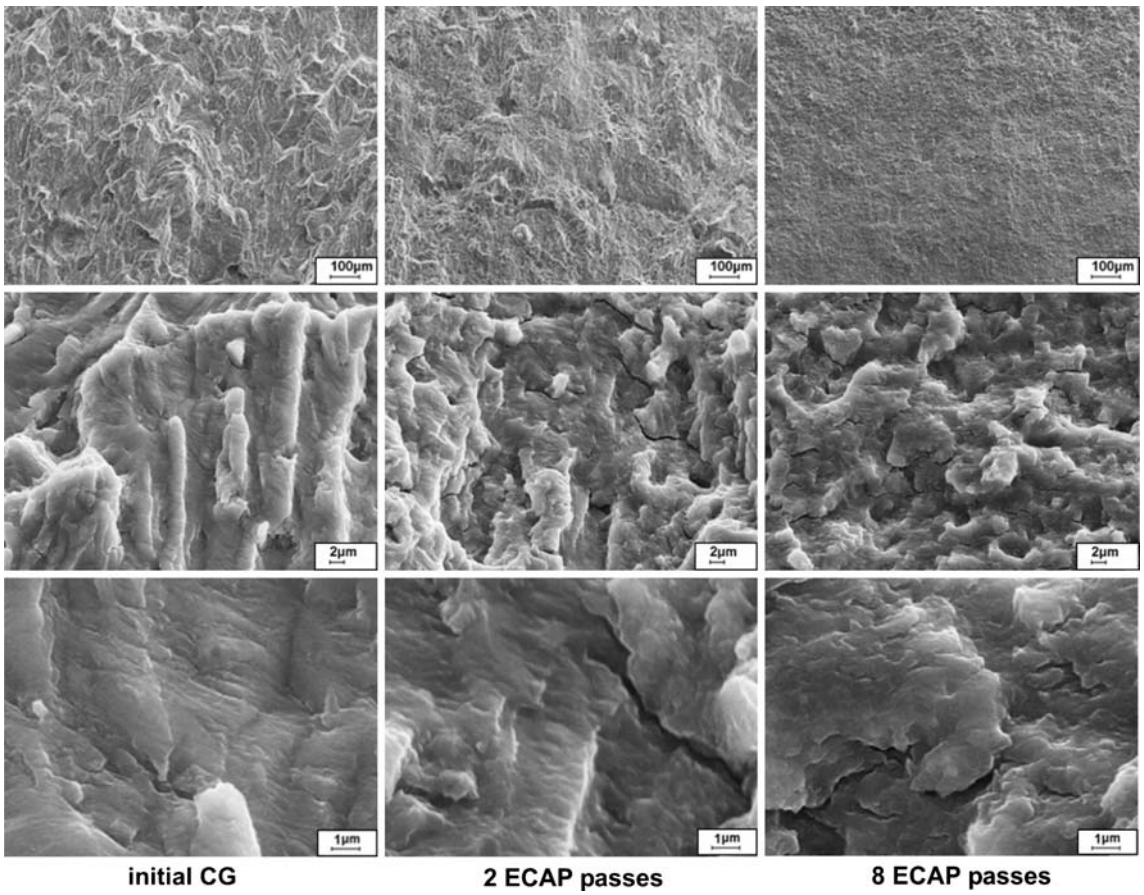

Fig. 5 SEM images of crack propagation surfaces at $\Delta K \approx 7$ MPam$^{1/2}$, direction of crack growth: ↑

a weaker cohesion in their lattice structure. Thus, it is assumed that the grain boundaries which are visible at the crack surfaces are most likely HABs.

When looking at the images of the crack surfaces taken with a lower magnification, strong differences in roughness can be detected, Fig. 5. The CG condition exhibits a rough and fissured surface, which indicates a strong deflection of the crack path along grain boundaries. After eight ECAP passes, the crack surface has a much smoother appearance. The bimodal condition represents a mixture of both morphologies, consisting of rough and smoother areas. As for a strongly deflected crack path, more energy is required for crack propagation, and the different grain sizes can be considered to be a crucial feature influencing the crack propagation.

Beyond that, also the material's ductility, in conjunction with its capability for strain hardening is supposed to be an important factor. Based on a model presented by Lukas and Gerberich [19] and discussed in [8], it is assumed that the fatigue threshold ΔK_{th} is lowered, amongst other factors, for a decrease in strain hardening capability. Especially at low stress intensities in the near-threshold region, mechanisms in the vicinity of the crack tip are in some way similar to those operating at LCF loading. Limited to slip bands emanating from the crack tip, dislocation movements take place and dislocations are impeded and piled up at obstacles such as (high angle) grain boundaries. As soon as the material's capability for strain hardening in those particular regions is exceeded, microcracks will occur, most likely at first in the weakest part of the microstructure. It is assumed that for the already severely strain hardened SPD conditions this results in a quite early initiation of microcracks, preferably either along a HAB (intergranular cracking) [8] or just within the slip band (transgranular cracking) [20].

For the SPD materials, the decrease in work hardening capability can clearly be seen in the stress–strain curves from the tensile test. Higher magnified micrographs of the crack surface in Fig. 5 reveal information on the material's ductility as well. Perpendicular to the direction of crack growth, microcracks are visible. For the SPD materials, those so-called secondary cracks appear longer and more straight-lined.

On the crack surface of the initial CG condition, striations perpendicular to the direction of crack growth can be detected. Those features indicate a rather ductile manner of crack propagation, associated with crack tip retardation and blunting [21]. For the bimodal condition, those striations are visible, too, though less pronounced. Additionally, characteristic secondary cracks can be found, emanating from valleys of the sawtooth-like striations. For the homogeneous UFG material after eight passes, numerous dendritic microcracks, supposably initiated along HABs, reveal a rather brittle manner of crack growth. Summarising these results it can be concluded that not only grain size and grain size distribution, but also ductility and microstructural factors such as grain boundary characteristics have an influence on fatigue crack growth properties.

Conclusions

Crack growth behaviour of AA6063 in the initial CG condition, a bimodal condition after two ECAP passes and a monomodal UFG condition after eight passes was investigated and related to microstructural and mechanical features. It was found that:

(1) The ECAP-processed materials exhibit higher crack growth rates and a lower fatigue threshold, when compared to the CG material. The bimodal condition shows an intermediate behaviour with tendency towards the homogeneous UFG condition.
(2) The crack growth rate and threshold behaviour are primarily attributed to grain sizes and grain size distribution, as it becomes obvious when looking at the roughness of the crack surfaces.
(3) Differences in distinctiveness of striations and patterns of secondary cracking reveal that other features such as strain hardening capability and grain boundary characteristics are also exerting an influence.

At this time, the major drawback of SPD materials in the as-processed condition is seen in their unfavourable LCF and fatigue crack growth properties, which are strongly limiting imaginable fields of practical application. From this point of view, new methods of combining ECAP and a subsequent heat treatment, which enables to regain the material's ductility to some extent, seem to be a promising method for paving the way for practical application [22–24].

Acknowledgements The authors thank the „Deutsche Forschungsgemeinschaft“ for supporting this research within the framework of „Sonderforschungsbereich 692“.

References

1. Valiev RZ, Islamgaliev RK, Alexandrov IV (2000) Prog Mater Sci 45:103. doi:10.1016/S0079-6425(99)00007-9
2. Horita Z, Fujinami T, Nemoto M, Langdon TG (2001) J Mater Process Tech 117:288. doi:10.1016/S0924-0136(01)00783-X
3. Höppel HW, Xu C, Kautz M, Barta-Schreiber N, Langdon TG, Mughrabi H (2004) In: Proc. of Int. Conf. Nanomaterials by Severe plastic deformation-NANOSPD. Wiley-VCH, Weinheim
4. Mughrabi H, Höppel HW, Kautz M (2004) Scripta Mater 51:807. doi:10.1016/j.scriptamat.2004.05.012
5. Vinogradov A, Washikita K, Kitagawa K, Kopylov VI (2003) Mater Sci Eng A 349:318. doi:10.1016/S0921-5093(02)00813-4
6. Patlan V, Vinogradov A, Higashi K, Kitagawa K (2001) Mater Sci Eng A 300:171. doi:10.1016/S0921-5093(00)01682-8

7. Vinogradov A, Nagasaki S, Patlan V, Kitagawa K, Kawazoe N (1999) Nanostruct Mater 11:925. doi:10.1016/S0965-9773(99)00392-X
8. Vinogradov A (2007) J Mater Sci 42:1797. doi:10.1007/s10853-006-0973-z
9. Chung CS, Kim JK, Kim HK, Kim WJ (2002) Mater Sci Eng A 337:39. doi:10.1016/S0921-5093(02)00010-2
10. Kießling R, Hübner P, Biermann H (2006) Materialprüfung 48:547
11. Turnbull A, de los Rios ER (1995) Fatigue Fract Eng Mater Struct 18:1355
12. Hockauf M, Meyer LW, Halle T, Kuprin C, Hietschold M, Schulze S et al (2006) Int J Mat Res 97:1392
13. Barber RE, Dudo T, Yasskin PB, Hartwig KT (2004) Scripta Mater 51:373. doi:10.1016/j.scriptamat.2004.05.022
14. Furukawa M, Horita Z, Langdon TG (2002) Mater Sci Eng A 332:97. doi:10.1016/S0921-5093(01)01716-6
15. ASTM Standard E 399-90, American Society for Testing and Materials
16. Watanabe T (1988) Mater Forum 11:284
17. Lim LC, Watanabe T (1990) Acta Metall Mater 38:2507. doi:10.1016/0956-7151(90)90262-F
18. Zhang ZF, Wang ZG (2000) Mater Sci Eng A 284:285. doi:10.1016/S0921-5093(00)00796-6
19. Lukas JP, Gerberich WW (1983) Fatigue Fract Eng Mater Struct 6:271
20. Zhang JZ (2000) Eng Fract Mech 65:665. doi:10.1016/S0013-7944(99)00148-4
21. Lynch SP (2007) Mater Sci Eng A 468–470:74. doi:10.1016/j.msea.2006.09.083
22. Höppel HW, Kautz M, Xu C, Muraskin M, Langdon TG, Valiev RZ et al (2006) Int J Fatigue 28:1001. doi:10.1016/j.ijfatigue.2005.08.014
23. Kim WJ, Wang JY (2007) Mater Sci Eng A 464:23. doi:10.1016/j.msea.2007.03.074
24. Hockauf M, Meyer LW, Zillmann B, Hietschold M, Schulze S, Krüger L (in press) Mater Sci Eng A